PHYSICAL REVIEW B **93**, 121403(R) (2016)

Temperature control of thermal radiation from composite bodies

Weiliang Jin,[1] Athanasios G. Polimeridis,[2] and Alejandro W. Rodriguez[1]
[1]*Department of Electrical Engineering, Princeton University, Princeton, New Jersey 08544, USA*
[2]*Skolkovo Institute of Science and Technology, Moscow, Russia*
(Received 1 July 2015; published 9 March 2016)

We demonstrate that recent advances in nanoscale thermal transport and temperature manipulation can be brought to bear on the problem of tailoring thermal radiation from wavelength-scale composite bodies. We show that such objects—complicated arrangements of phase-change chalcogenide ($Ge_2Sb_2Te_5$) glasses and metals or semiconductors—can be designed to exhibit strong resonances and large temperature gradients, which in turn lead to large and highly directional emission at midinfrared wavelengths. We find that partial directivity depends sensitively on a complicated interplay between shape, material dispersion, and temperature localization within the objects, requiring simultaneous design of the electromagnetic scattering and thermal properties of these structures. Our calculations exploit a recently developed fluctuating-volume current formulation of electromagnetic fluctuations that rigorously captures radiation phenomena in structures with strong temperature and dielectric inhomogeneities, such as those studied here.

DOI: 10.1103/PhysRevB.93.121403

Introduction. The ability to control thermal radiation over selective frequencies and angles through complex materials and nanostructured surfaces [1] has enabled unprecedented advances in important technological areas, including remote temperature sensing [2], incoherent sources [3,4], and energy harvesting [5–7]. While unusual radiation patterns, e.g., spatial coherence and directivity, have been recently demonstrated in photonic crystals [1,7–9], metamaterials [10–13], and large-etalon structures composed of partially transparent materials [14], the design of temperature distributions in composite structures with features on the scale of the thermal wavelength (for enhanced emission) appears largely unexplored. Such an approach combines both nanophotonic and conductive design principles and is poised to take advantage of recent progress in the areas of temperature management and heat transport at submicron scales [15,16].

In this Rapid Communication, we exploit a recently proposed fluctuating-volume current (FVC) formulation of electromagnetic (EM) fluctuations in inhomogeneous media to demonstrate that when selectively heated, wavelength-scale composite bodies—complicated arrangements of phase-change materials and metals or semiconductors—can exhibit large temperature gradients that enable designable, directional emission at infrared wavelengths. Specifically, we show that micron-scale chalcogenide [$Ge_2Sb_2Te_5$ (GST)] hemispheroids coated with titanium or silicon-nitride shells (Fig. 1) and resting on low-index, transparent substrates, can exhibit large emissivity and $\gtrsim 80\%$ partial directivity. This effect is a consequence of a dual radiation/conduction design strategy that achieves both resonance enhancement and temperature localization within the GST, the interplay of which enables these composite infrared thermal antennas to not only enhance but also selectively emit/absorb light in specific directions. Temperature localization is important for achieving directional emission and is attained by the heating of a highly conductive two-dimensional (2D) material at the GST-substrate interface, whose radiation is redirected either away or toward the metallic or semiconducting shells, respectively. We show that anisotropic emission depends sensitively on geometry but can arise in a wide range of composite objects, including mushroomlike particles and coated cylinders, while it is absent in homogeneous or composite objects under uniform temperature distributions. Our predictions are based on accurate numerical solutions of the conductive heat equation and Maxwell's equations, which not only incorporate material dispersion but also account for the existence of thermal and dielectric gradients at the scale of the EM wavelength, where ray optical descriptions are inapplicable.

Attempts to obtain unusual thermal radiation patterns have primarily relied on Bragg scattering and related interference effects in nanostructured surfaces [1], including photonic gratings [7–9], metasurfaces [17–24], multilayer structures [25–28], and subwavelength metamaterials [6,11–13]. Related ideas can also be found in the context of fluorescence emission, where directivity is often achieved by employing metallic objects (e.g., plasmonic antennas) to redirect emission from individual dipolar emitters via gratings [29,30] or by localizing fluorescent molecule(s) to within some region in the viscinity of an external scatterer [31–36]. Matters become complicated when the emission is coming from random sources distributed within a wavelength-scale object, as is the case for thermal radiation, because the relative contribution of current sources to radiation in a particular direction is determined by both the shape and temperature distribution of the object. Optical antennas have recently been proposed as platforms for control and design of narrowband emitters [37,38], though predictions of large directivity continue to be restricted to periodic structures. While there is increased focus on the study of light scattering from subwavelength particles and microwave antennas (useful for radar detection [39], sensing [40], and color routing [41,42]), similar ideas have yet to be translated to the problem of thermal radiation from compact, wavelength-scale objects, whose radiation is typically quasi-isotropic [1]. Here, we show that temperature manipulation in composite particles could play an important role in the design of coherent thermal emitters.

Temperature gradients can arise near the interface of materials with highly disparate thermal conductivities [16]. Although often negligible at macroscopic scales [43], recent experiments reveal that the presence of thermal boundary

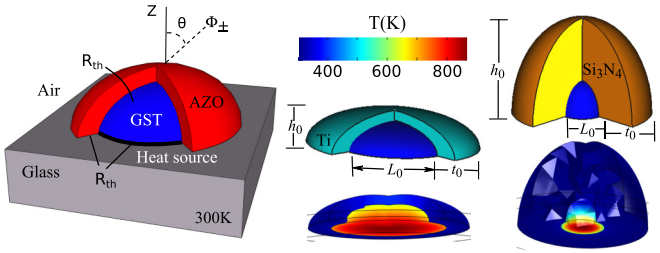

FIG. 1. Schematic of two composite bodies, involving GST (blue) hemispheroids coated with Ti (green), AZO (red), or Si_3N_4 (orange) shells, which rest on a low-index, transparent substrate in contact with a heat reservoir at 300 K. The GST is heated from below by a conductive 2D material (e.g., a carbon-nanotube wall or graphene sheet), leading to temperature gradients within the structure. The presence of boundary resistance at material interfaces is captured by effective thermal resistances (see text). Figure 2 explores radiation from GST-Ti and GST-Si_3N_4 bodies with parameters $L_0 = 1.7\ \mu$m, $t_0 = 0.3\ \mu$m, $h_0 = 0.5\ \mu$m and $L_0 = 1.3\ \mu$m, $t_0 = 1.3\ \mu$m, $h_0 = 2.6\ \mu$m, respectively, and under various heating conditions (see text); here we show the temperature profile corresponding to scenario (iii).

resistance [44,45] (including intrinsic and contact resistance [46]) in nanostructures together with large dissipation can enable temperature localization over small distances [43]. Such temperature control has been recently investigated in the context of metallic nanospheres immersed in fluids [47], graphene transistors [48], nanowire resistive heaters [49], atomic force microscope tips [50], and magnetic contacts [51]. With the exception of a few high-symmetry structures, e.g., spheres [52] and planar films [28], however, calculations of thermal radiation from wavelength-scale bodies have been restricted to uniform-temperature operating conditions, exploiting Kirchoff's law [28,53] to obtain radiative emission via simple scattering calculations.

Formulation. In what follows, we present a brief derivation of our FVC formulation of thermal radiation for inhomogeneous media, with validations and details of its numerical implementation described in a separate paper [54]. Our starting point is the volume-integral equations (VIE) formulation of EM scattering [55], describing scattering of an incident, six-component electric (**E**) and magnetic (**M**) field $\phi_{\rm inc} = (\mathbf{E};\mathbf{H})$ from a body described by a spatially varying 6×6 susceptibility tensor $\chi(\mathbf{x})$. (For convenience, we omit the frequency ω dependence of material properties, currents, fields, and operators.) Given a six-component electric (**J**) and magnetic (**M**) dipole source $\sigma = (\mathbf{J};\mathbf{M})$, the incident field is obtained via a convolution ($\star$) with the 6×6 homogeneous Green's function of the ambient medium $\Gamma(\mathbf{x},\mathbf{y})$, such that $\phi_{\rm inc} = \Gamma\star\sigma = \int d^3\mathbf{y}\,\Gamma(\mathbf{x},\mathbf{y})\sigma(\mathbf{y})$. Exploiting the volume equivalence principle [55], the unknown scattered fields $\phi_{\rm sca} = \Gamma\star\xi$, can also be expressed via convolutions with Γ, except that here $\xi = -i\omega\chi\phi$ are the (unknown) bound currents in the body, related to the total field inside the body $\phi = \phi_{\rm inc} + \phi_{\rm sca}$ through χ. Writing Maxwell's equations in terms of the incident and induced currents,

$$\xi + i\omega\chi(\Gamma\star\xi) = -i\omega\chi(\Gamma\star\sigma), \qquad (1)$$

one obtains ξ in terms of the incident source σ.

The standard approach to numerically solve Eq. (1) is to consider expansion of the current sources $\sigma(\mathbf{x}) = \sum_n s_n b_n(\mathbf{x})$ and $\xi(\mathbf{x}) = \sum_n x_n b_n(\mathbf{x})$ in a convenient, orthonormal basis $\{b_n\}$ of N six-component vectors, with vector coefficients s and x, respectively. The resulting matrix expression has the form $x + s = Ws$, where $(W^{-1})_{m,n} = \langle b_m, b_n + i\omega\chi(\Gamma\star b_n)\rangle$ is known as the VIE matrix and $\langle,\rangle$ denotes the standard conjugated inner product. Direct application of Poynting's theorem then yields the far-field radiation flux $\Phi = \frac{1}{2}\,\mathrm{Re}\int d^3\mathbf{x}\,(\mathbf{E}^*\times\mathbf{H}) = -\frac{1}{2}\,\mathrm{Re}\,\xi^*\phi$ due to σ in terms of the VIE operators [56]:

$$\Phi = -\tfrac{1}{2}\mathrm{Tr}[C\,W^*\,\mathrm{sym}\,GW], \qquad (2)$$

where we have defined the current-current correlation matrix C, whose elements $C_{mn} = \langle s_m s_n^*\rangle = \iint d^3\mathbf{x}\,d^3\mathbf{y}\,b_m^*(\mathbf{x})\langle\sigma(\mathbf{x})\sigma^*(\mathbf{y})\rangle b_n(\mathbf{y})$. The correlation functions satisfy a well-known fluctuation-dissipation theorem [57], $\langle\sigma_i(\mathbf{x},\omega)\sigma_j^*(\mathbf{y},\omega)\rangle = \frac{4}{\pi}\omega\ \mathrm{Im}\,\chi(\mathbf{x},\omega)\Theta(\mathbf{x},\omega)\delta(\mathbf{x}-\mathbf{y})\delta_{ij}$, relating current fluctuations to the dissipative $\sim\mathrm{Im}\,\chi$ and thermodynamic properties of the underlying materials. Here, $\Theta(\mathbf{x},\omega) = \hbar\omega/(e^{\hbar\omega/k_{\rm B}T(\mathbf{x})} - 1)$ is the Planck distribution at the local temperature $T(\mathbf{x})$ [58]. One can also obtain a similar trace expression for the angular radiation flux in a given direction, as shown in [54]. Equation (2) can be employed to calculate emission from arbitrarily shaped bodies with spatially varying dielectric and temperature properties: unlike previous scattering-matrix and surface-integral equation formulations of thermal radiation [58], the FVC scattering unknowns are volumetric currents.

Tailoring emission. We explore radiation from composite bodies comprised of chalcogenide $Ge_2Sb_2Te_5$ (GST) alloys and metals or semiconductors. To begin with, we consider micron-scale GST hemispheroids coated with either titanium (Ti) or silicon-nitride (Si_3N_4) shells, depicted in Fig. 1. The structures rest on a low-index ($\varepsilon\approx 1$) transparent substrate which not only provides mechanical support but also a means of dissipating heat away from the structure; the bottom of the substrate is assumed to be in contact with a 300 K heat reservoir, while surfaces exposed to vacuum satisfy adiabatic boundary conditions ($\nabla T\cdot\hat{\mathbf{n}} = 0$). When heated by a highly conductive 2D material (e.g., by applying current through a carbon nanotube wall [59] or graphene sheet) at the GST-substrate interface, such a structure can exhibit large temperature gradients within the core, a consequence of boundary resistance [44–47] between the various interfaces and rapid heat dissipation in the highly conductive shells [44,59,60]. To model the corresponding steady-state temperature distribution $T(\mathbf{x})$, we solve the heat-conduction equation via COMSOL [61], including the full temperature-dependent thermal conductivity $\kappa(T)$ of the GST [62]. Note that even at large temperatures, $\kappa_{\rm GST}(800\ {\rm K}) \ll \kappa_{\rm Ti,Si_3N_4}(300\ {\rm K}) \gtrsim 20\ {\rm W/mK}$. The existence of thermal boundary resistance [46,63] at this scale is taken into account by the introduction of effective resistances $R_{\rm sh|c}$, $R_{\rm h|su}$, and $R_{\rm sh|su}$, at the interfaces between shell-GST, heater-substrate, and shell-substrate, respectively [see Supplemental Material (SM) [64]]. Figure 1 shows $T(\mathbf{x})$ throughout the Ti structure when the GST-substrate interface is heated to $T_{\rm GST} = 870$ K (approaching the GST melting temperature [65] and corresponding to a thermal wavelength $\lambda_T \approx hc/2.8k_{\rm B}T \approx 5.8\ \mu$m), and under various operating conditions. We consider

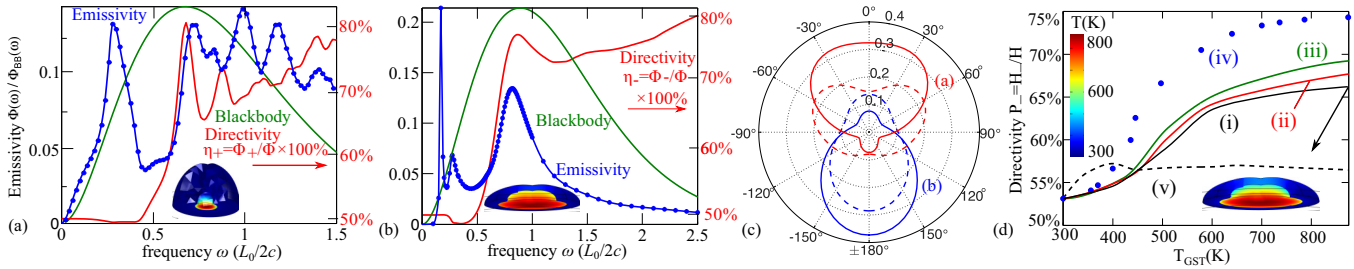

FIG. 2. Spectral emissivity $\epsilon(\omega) = \Phi(\omega)/\Phi_{\rm BB}(\omega)$ (blue dots) from heterogeneous bodies comprising $Ge_2Sb_2Te_5$ (GST) hemispheroids coated with either (a) Si_3N_4 or (b) Ti shells and resting on a low-index substrate (object dimensions are specificed in Fig. 1). The structures are heated from the GST-substrate interface by a 2D thin-film conductor under heating scenario (iii), described in the text, with an interface temperature $T_{\rm GST} = 870$ K. The resulting temperature profiles $T(\mathbf{x})$ are shown in Fig. 1 and in the insets. ϵ is defined as the ratio of the thermal flux $\Phi(\omega)$ of each body normalized to the flux $\Phi_{\mathbf{BB}} = \frac{A}{4\pi^2}(\omega/c)^2\Theta(\omega,T)$ from a corresponding blackbody of the same surface area A but uniform $T = 870$ K (green lines, arb. units). Also shown are the partial directivities $\eta_\pm = \Phi_\pm/\Phi$ (red line), defined as the ratios of the outgoing flux into the upper/lower hemisphere $\Phi_\pm = 2\pi\int_{\mp\pi/2}^{\pi\mp\pi/2} d\theta\,\Phi(\omega,\theta)$ to the total flux, where θ is defined in Fig. 1. (c) Angular radiation intensity $\Phi(\theta)$ normalized by the total flux Φ, for the structures in (a) (solid red line) and (b) (solid blue line) under scenario (iii), compared to emission under uniform-temperature conditions (dashed lines). (d) Total (frequency-integrated) partial directivity $P_- = H_-/H$ as a function of $T_{\rm GST}$, with $H_- = \int d\omega\,\Phi_-$, for the Ti structure under different heating conditions, corresponding to multiple degrees of temperature localization in the GST (see text).

$R_{\rm sh|su} = 10^{-8}$ m^{2}W/K [44] and $R_{\rm sh|c} = R_{\rm h|su} = R_{th}$, with (i), (ii), and (iii) corresponding to typical values of $R_{th} = \{0.5,1,2\}\times 10^{-7}$ m^{2}W/K [44] while (iv) $R_{\rm th} = \infty$ and (v) $R_{\rm th} = 0$ describe either perfect temperature localization in the GST or uniform temperature throughout the structure, respectively. (Note that the values of boundary resistance associated with a given experimental realization of these composites will depend on the specific choice of fabrication technique and materials.) In what follows, we exploit $T(\mathbf{x})$, Eq. (2), and the dielectric properties of these materials (taking into account material dispersion) [66–69], to obtain the flux from these composites. Note that due to large temperature gradients and phase transitions in the GST [62], its dielectric response $\varepsilon_{\rm GST}[T(\mathbf{x}),\omega]$ consists of continuously varying rather than piecewise constant regions (SM); our FVC method, however, can handle arbitrarily varying $\varepsilon(\mathbf{x})$ and $T(\mathbf{x})$. (Note that the temperature inside the Ti and Si_3N_4 shells is roughly 300 K.)

Figure 2 shows the emissivity (blue dots) and partial directivity (solid lines) of the (a) Si_3N_4 and (b) Ti structures, along with the corresponding $T(\mathbf{x})$ (insets) under heating scenario (iii), assuming $T_{\rm GST} = 870$ K. The emissivity $\epsilon(\omega) = \Phi(\omega)/\Phi_{\rm BB}(\omega)$ is defined as the ratio of the thermal flux $\Phi(\omega)$ from each object to that of a blackbody $\Phi_{\rm BB}(\omega) = \frac{A}{4\pi^2}(\omega/c)^2\Theta(\omega,T)$ of the same *overall* surface area A and $T = 870$ K (green lines); the partial directivity $\eta_\pm = \Phi_\pm/\Phi$ is defined as the ratio of the flux into the upper/lower hemisphere $\Phi_\pm(\omega) = 2\pi\int_{\mp\pi/2}^{\pi\mp\pi/2} d\theta\,\Phi(\omega,\theta)$, to the total flux Φ, where θ is defined with respect to the $+\hat{z}$ axis (Fig. 1). As expected, ϵ displays enhanced emission at geometric resonances, with peak magnitudes $\epsilon \lesssim 0.2$ limited by material losses (Im $\varepsilon \lesssim$ Re ε) in this frequency range [70]. (Larger ϵ can likely be obtained with further design or other material combinations.) Also notable is the sharp increase in η as the emission regime changes from quasistatic to wavelength scale: despite the temperature localization, at low $\omega L/c \ll 1$ the emission is quasi-isotropic (as expected from a randomly polarized dipolar emitter [17]). In contrast, one finds that with increasing $\omega L/c \gtrsim 1$ and with the help of the curvature [14], the Si_3N_4 and Ti shells increasingly redirect radiation upwards or downwards as a result of *coherent* interference between the radiated and scattered fields. Such strong directional scattering is absent from dipole fluctuations originating in the shells, which tend to radiate isotropically and dominate emission, making the design of the temperature profile an essential ingredient for achieving large η. Figure 2(c) illustrates this point by showing the angular radiation intensity $\Phi(\theta)$ of the Si_3N_4 (red) and Ti (blue) structures at selected frequencies, under two of the heating conditions, corresponding to either (ii) partial temperature localization in the GST (solid lines) or (v) uniform temperature throughout the bodies (dashed lines). The dependence of radiation on $T(\mathbf{x})$ is further explored in Fig. 2(d), which shows the total (frequency-integrated) partial directivity $P_- = H_-/H$ of the Ti structure under different $T_{\rm GST}$ and heating conditions, where $H_\pm = \int_0^\infty d\omega\,\Phi_\pm$. As shown, P_- increases with increasing temperature localization (attained at larger $T_{\rm GST}$), and remains almost constant, $P_- \approx 0.5$, under uniform-temperature conditions. Such an increase in partial directivity, however, comes at the expense of smaller ϵ (not shown), a consequence of the increasingly dominant role of higher frequencies which suffer from larger material losses.

Our choice of shapes and materials for these composites ensure large ϵ and η at selective wavelengths $\omega L/c \sim 1$, dictated by our choice of operating temperature and satisfying the following general design criteria: (i) cold (scatterer) and hot (emitter) regions with large and small κ, respectively, in order to achieve and maintain a large temperature differential; (ii) hot regions with large Re ϵ and small losses supporting strong resonances near λ_T; (iii) large index contrasts and optimal shapes/sizes leading to high thermal extraction/reflections from hot regions and thus large directivity. GST/Ti/Si_3N_4 material combinations partially satisfy these conditions, since $\varepsilon_{\rm GST} \approx 30 + 5i$ [66,67], $\varepsilon_{\rm Ti} \approx -100 + 80i$ [68], and $\varepsilon_{\rm Si_3N_4} \approx 5 + 0.1i$ [69] at midinfrared wavelengths $\lambda_T \approx 5.8$ μm. Optimal shapes for achieving directional emission depend strongly

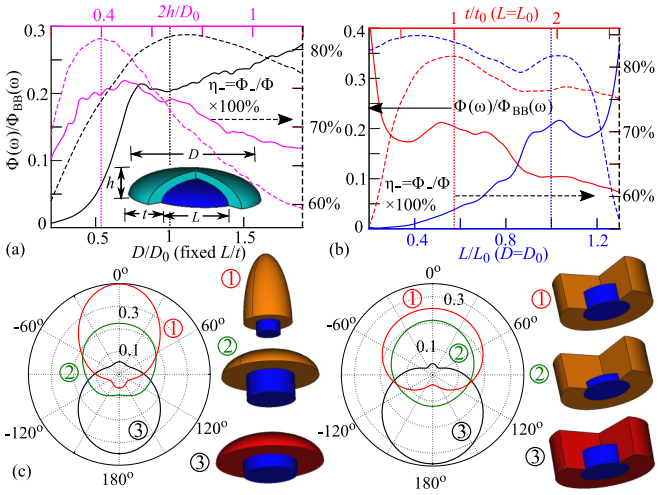

FIG. 3. (a), (b) Peak directivity η_- (dashed lines, right axes) and emissivity ϵ (solid lines, left axes) associated with the resonance closest to the peak of the BB spectrum of Ti-shell hemispheroids (Fig. 1) as a function of various shape/size parameters, including aspect ratio $2h/D$ (magenta), overall size D (black), metal thickness t with a fixed GST size $L = L_0$ (red), and GST size L with a fixed overall size $D = D_0$ (blue). Here, the subscripts "0" and the vertical dashed lines denote size parameters specified in Fig. 1. (c) Angular radiation intensity $\Phi(\theta)$ from various heterogeneous bodies—composite GST (blue), AZO (red), and Si_3N_4 (orange) mushrooms and cylinders—at selected frequencies ω and normalized by the total flux Φ. All plots assume perfect $T = 870$ K localization in the GST, while other materials are held at 300 K.

on the choice of hot/cold material and operating temperature: we find that GST-Si_3N_4 composites favor large-curvature prolate structures, while GST-Ti/AZO composites favor oblate structures, ensuring increased extraction and reflections from the shells, respectively.

Figures 3(a) and 3(b) illustrate the sensitive relationship between shape and emission for the GST-Ti structure under heating scenario (iv), with the GST and Ti regions held at 870 and 300 K, respectively. Shown are the peak η_- (dashed lines, right axes) and ϵ (solid lines, left axes) associated with the resonance closest to the peak of the blackbody (BB) spectrum, as a function of various geometric parameters, including (i) aspect ratio $2h/D$ (magenta line), demonstrating that directivity is maximized at a specific aspect ratio ≈ 0.4 and thus validating our previous observation that oblate objects ($2h/D < 1$) tend to maximize directivity in this configuration; (ii) overall object size D with all other parameters fixed (black line), showing that there exists an optimal D_0, due mainly to material dispersion; (iii) Ti thickness t with fixed GST size L_0 (red line), showing that there is an optimal shell thickness (t_0) which maximizes reflections (note that as t increases, ϵ decreases due to larger metal losses); and (iv) GST size L with a fixed overall size D_0 (blue line), showing two optimal values of $L = 0.4L_0$ and $1.1L_0$, with the former exhibiting slightly larger η_- but leading to lower emissivity: $\epsilon \to 0$ as $L \to 0$ due to increased radiative losses. These results illustrate the dramatically different design criteria associated with wavelength- versus large-scale bodies (where emission is bounded by ray-optical limits [71]). For instance, while larger η_- can be attained in the ray-optics limit by increasing the shell thicknesses relative to the core dimensions (thereby enhancing extraction/reflections from the GST), this would also result in lower ϵ. Wavelength-scale structures not only provide a high degree of temperature and emission control, but enable simultaneous enhancement in η and ϵ with the latter potentially exceeding the blackbody limit [70]. Figure 3(c) shows radiation patterns from other composite shapes (details of which can be found in the SM), including mushroomlike particles, and cylinders (blue/red/orange denote GST/AZO/Si_3N_4), at selective ω and under heating scenario (iv), demonstrating a high degree of emission tunability.

Concluding remarks. Our predictions above provide just a glimpse of the interesting phenomena that can arise in structures that combine conductive and radiative design principles. While our focus here is on compact objects (micron/nano composite antennas), extensions to periodic structures are also feasible within the same framework, requiring minor modifications [72] and potentially enabling even further radiation control.

[1] J.-J. Greffet and C. Henkel, Contemp. Phys. **48**, 183 (2007).
[2] K. Masuda, T. Takashima, and Y. Takayama, Remote Sens. Environ. **24**, 313 (1988).
[3] O. Ilic and M. Soljačić, Nat. Mater. **13**, 920 (2014).
[4] V. Rinnerbauer, A. Lenert, D. M. Bierman, Y. X. Yeng, W. R. Chan, R. D. Geil, J. J. Senkevich, J. D. Joannopoulos, E. N. Wang, M. Soljačić *et al.*, Adv. Energy Mater. **4**, 1400334 (2014).
[5] S. Fan, Nat. Nanotechnol. **9**, 92 (2014).
[6] P. Bermel, M. Ghebrebrhan, M. Harradon, Y. X. Yeng, I. Celanovic, J. D. Joannopoulos, and M. Soljacic, Nanoscale Res. Lett. **6**, 1 (2011).
[7] M. Florescu, H. Lee, I. Puscasu, M. Pralle, L. Florescu, D. Z. Ting, and J. P. Dowling, Sol. Energy Mater. Sol. Cells **91**, 1599 (2007).
[8] M. De Zoysa, T. Asano, K. Mochizuki, A. Oskooi, T. Inoue, and S. Noda, Nat. Photonics **6**, 535 (2012).
[9] W. Wang, C. Fu, and W. Tan, J. Quant. Spectrosc. Radiat. Transfer **132**, 36 (2014).
[10] D. Ding and A. J. Minnich, Opt. Express **23**, A299 (2015).
[11] B. Lee, L. Wang, and Z. Zhang, Opt. Express **16**, 11328 (2008).
[12] C. Fu and Z. M. Zhang, Front. Energy Power Eng. China **3**, 11 (2009).
[13] X. Liu, T. Tyler, T. Starr, A. F. Starr, N. M. Jokerst, and W. J. Padilla, Phys. Rev. Lett. **107**, 045901 (2011).
[14] Z. Yu, N. P. Sergeant, T. Skauli, G. Zhang, H. Wang, and S. Fan, Nat. Commun. **4**, 1730 (2013).
[15] D. G. Cahill, W. K. Ford, K. E. Goodson, G. D. Mahan, A. Majumdar, H. J. Maris, R. Merlin, and S. R. Phillpot, J. Appl. Phys. **93**, 793 (2003).

[16] D. G. Cahill, P. V. Braun, G. Chen, D. R. Clarke, S. Fan, K. E. Goodson, P. Keblinski, W. P. King, G. D. Mahan, A. Majumdar *et al.*, Appl. Phys. Rev. **1**, 011305 (2014).
[17] J.-J. Greffet, R. Carminati, K. Joulain, J.-P. Mulet, S. Mainguy, and Y. Chen, Nature (London) **416**, 61 (2002).
[18] F. Marquier, K. Joulain, J.-P. Mulet, R. Carminati, J.-J. Greffet, and Y. Chen, Phys. Rev. B **69**, 155412 (2004).
[19] K. Joulain, J.-P. Mulet, F. Marquier, R. Carminati, and J.-J. Greffet, Surf. Sci. Rep. **57**, 59 (2005).
[20] P. J. Hesketh, J. N. Zemel, and B. Gebhart, Phys. Rev. B **37**, 10803 (1988).
[21] A. Narayanaswamy and G. Chen, J. Quant. Spectrosc. Radiat. Transfer **93**, 175 (2005).
[22] F. Marquier, D. Costantini, A. Lefebvre, A.-L. Coutrot, I. Moldovan-Doyen, J.-P. Hugonin, S. Boutami, H. Benisty, and J.-J. Greffet, in *SPIE OPTO* (International Society for Optics and Photonics, San Francisco, CA, 2015), pp. 937004–937004.
[23] V. Kleiner, N. Dahan, K. Frischwasser, and E. Hasman, in *SPIE OPTO* (International Society for Optics and Photonics, San Francisco, CA, 2012), pp. 82700R–82700R.
[24] T. Ribaudo, D. W. Peters, A. R. Ellis, P. S. Davids, and E. A. Shaner, Opt. Express **21**, 6837 (2013).
[25] O. Kollyukh, A. Liptuga, V. Morozhenko, and V. Pipa, Opt. Commun. **225**, 349 (2003).
[26] P. Ben-Abdallah, J. Opt. Soc. Am. A **21**, 1368 (2004).
[27] J. Drevillon, K. Joulain, P. Ben-Abdallah, and E. Nefzaoui, J. Appl. Phys. **109**, 034315 (2011).
[28] L. Wang, S. Basu, and Z. Zhang, J. Heat Transfer **133**, 072701 (2011).
[29] A. G. Curto, G. Volpe, T. H. Taminiau, M. P. Kreuzer, R. Quidant, and N. F. van Hulst, Science **329**, 930 (2010).
[30] T. Kosako, Y. Kadoya, and H. F. Hofmann, Nat. Photonics **4**, 312 (2010).
[31] T. V. Teperik and A. Degiron, Phys. Rev. B **83**, 245408 (2011).
[32] M. Thomas, J.-J. Greffet, R. Carminati, and J. Arias-Gonzalez, Appl. Phys. Lett. **85**, 3863 (2004).
[33] C. Li, G. W. Kattawar, Y. You, P. Zhai, and P. Yang, J. Quant. Spectrosc. Radiat. Transfer **106**, 257 (2007).
[34] C. Vandenbem, L. Froufe-Pérez, and R. Carminati, J. Opt. A: Pure Appl. Opt. **11**, 114007 (2009).
[35] C. Vandenbem, D. Brayer, L. S. Froufe-Pérez, and R. Carminati, Phys. Rev. B **81**, 085444 (2010).
[36] A. Mohammadi, V. Sandoghdar, and M. Agio, New J. Phys. **10**, 105015 (2008).
[37] J. A. Schuller, T. Taubner, and M. L. Brongersma, Nat. Photonics **3**, 658 (2009).
[38] L. Novotny and N. Van Hulst, Nat. Photonics **5**, 83 (2011).
[39] C. A. Balanis, *Antenna Theory: Analysis and Design* (Wiley, New York, 2005), Vol. 1.
[40] T. H. Taminiau, R. J. Moerland, F. B. Segerink, L. Kuipers, and N. F. van Hulst, Nano Lett. **7**, 28 (2007).
[41] S. Alavi Lavasani and T. Pakizeh, J. Opt. Soc. Am. B **29**, 1361 (2012).
[42] T. Shegai, S. Chen, V. D. Miljković, G. Zengin, P. Johansson, and M. Käll, Nat. Commun. **2**, 481 (2011).
[43] A. A. Balandin, Nat. Mater. **10**, 569 (2011).
[44] J. P. Reifenberg, D. L. Kencke, and K. E. Goodson, IEEE Electron Device Lett. **29**, 1112 (2008).
[45] A. M. Marconnet, M. A. Panzer, and K. E. Goodson, Rev. Mod. Phys. **85**, 1295 (2013).
[46] R. J. Stevens, L. V. Zhigilei, and P. M. Norris, Int. J. Heat Mass Transfer **50**, 3977 (2007).
[47] S. Merabia, P. Keblinski, L. Joly, L. J. Lewis, and J.-L. Barrat, Phys. Rev. E **79**, 021404 (2009).
[48] S. Islam, Z. Li, V. E. Dorgan, M.-H. Bae, and E. Pop, IEEE Electron Device Lett. **34**, 166 (2013).
[49] J. Yeo, G. Kim, S. Hong, J. Lee, J. Kwon, H. Lee, H. Park, W. Manoroktul, M.-T. Lee, B. J. Lee *et al.*, Small **10**, 5014 (2014).
[50] W. P. King, B. Bhatia, J. R. Felts, H. J. Kim, B. Kwon, B. Lee, S. Somnath, and M. Rosenberger, Annu. Rev. Heat Transfer **16**, 287 (2013).
[51] S. Petit-Watelot, R. M. Otxoa, M. Manfrini, W. Van Roy, L. Lagae, J.-V. Kim, and T. Devolder, Phys. Rev. Lett. **109**, 267205 (2012).
[52] L. A. Dombrovsky, Int. J. Heat Mass Transfer **43**, 1661 (2000).
[53] C. Luo, A. Narayanaswamy, G. Chen, and J. D. Joannopoulos, Phys. Rev. Lett. **93**, 213905 (2004).
[54] A. G. Polimeridis, M. Reid, W. Jin, S. G. Johnson, J. K. White, and A. W. Rodriguezz, Phys. Rev. B **92**, 134202 (2015).
[55] A. Polimeridis, J. Villena, L. Daniel, and J. White, J. Comput. Phys. **269**, 280 (2014).
[56] W. C. Chew, J. Jian-Ming, E. Michielssen, and S. Jiming, *Fast and Efficient Algorithms in Computational Electromagnetics* (Artech, Norwood, MA, 2001).
[57] L. D. Landau, E. M. Lifshitz, and L. P. Pitaevskiĭ, *Statistical Physics Part 2* (Pergamon, Oxford, 1960), Vol. 9.
[58] A. W. Rodriguez, M. T. H. Reid, and S. G. Johnson, Phys. Rev. B **88**, 054305 (2013).
[59] F. Xiong, A. Liao, and E. Pop, Appl. Phys. Lett. **95**, 243103 (2009).
[60] J. Liang, R. G. D. Jeyasingh, H.-Y. Chen, and H. Wong, IEEE Trans. Electron Devices **59**, 1155 (2012).
[61] Note that at these temperatures convective and radiative effects are negligible compared to conductive transfer, allowing us to consider the radiation and conduction problems separately.
[62] H.-K. Lyeo, D. G. Cahill, B.-S. Lee, J. R. Abelson, M.-H. Kwon, K.-B. Kim, S. G. Bishop, and B.-k. Cheong, Appl. Phys. Lett. **89**, 151904 (2006).
[63] J. Holman, *Heat Transfer*, Interntional ed. (McGraw-Hill, New York, 2009).
[64] See Supplemental Material at http://link.aps.org/supplemental/10.1103/PhysRevB.93.121403 for details of geometric, material properties, and heating schemes.
[65] T. Tsafack, E. Piccinini, B.-S. Lee, E. Pop, and M. Rudan, J. Appl. Phys. **110**, 063716 (2011).
[66] K. Shportko, S. Kremers, M. Woda, D. Lencer, J. Robertson, and M. Wuttig, Nat. Mater. **7**, 653 (2008).
[67] X. Z. Li, J. K. Choi, Y. S. Byun, S. Y. Kim, K. S. Sim, and S. K. Kim, Jpn. J. Appl. Phys. **47**, 5477 (2008).
[68] I. Mash and G. Motulevich, Sov. Phys. JETP **36**, 526 (1973).
[69] J. Kischkat, S. Peters, B. Gruska, M. Semtsiv, M. Chashnikova, M. Klinkmüller, O. Fedosenko, S. Machulik, A. Aleksandrova, G. Monastyrskyi *et al.*, Appl. Opt. **51**, 6789 (2012).
[70] C. F. Bohren and D. R. Huffman, *Absorption and Scattering of Light by Small Particles* (Wiley, New York, 2008).
[71] M. Weinstein, Am. J. Phys. **28**, 123 (1960).
[72] L. Greengard, K. L. Ho, and J.-Y. Lee, J. Comput. Phys. **258**, 738 (2014).